Modeling Aboveground Biomass Using Non-Redundant Vegetation Indices from PlanetScope Imagery via Multiple Linear Regression in Planted Forests

Sarono. [1*], Erna Kurniati[2]

[1]Doctoral Program in Geography, Faculty of Geography, Universitas Gadjah Mada,

Yogyakarta, Indonesia.

[2] Post-Graduated of Remote Sensing, Faculty of Geography, Universitas Gadjah Mada,

Yogyakarta,Indonesia.

*sarono90@mail.ugm.ac.id

Abstract : *Aboveground biomass (AGB) estimation using vegetation indices (VIs) derived from high-resolution satellite imagery has been widely applied, yet its accuracy often varies depending on the spectral characteristics of each index. This study aims to improve AGB estimation by combining non-redundant VIs selected through Pearson Correlation Matrix (PCM) analysis, applied to PlanetScope SuperDove imagery in the Wanagama Forest, Yogyakarta, Indonesia. A total of 18 VIs were calculated and screened using PCM on 404 sample points, with indices classified into redundancy groups. Eight single indices were identified as candidates, while multi-index combinations were constructed using two schemes: mixed combinations without correlation sign separation, and separated combinations distinguishing positive and negative correlations. Biomass estimation was performed using Simple Linear Regression (SLR) for single indices and Multiple Linear Regression (MLR) for multi-index models, with 70% of field-measured AGB samples (n = 137) used for training and 30% (n = 63) for validation. Results showed that model performance varied considerably across scenarios. Among single indices, GNDVI achieved the highest accuracy ($R^2 = 0.48$), reflecting the strong role of NIR in capturing canopy structure. For multi-index models, Com1– (GNDVI–CIVE–MGRVI–RGR–BGR) yielded the best performance with $R = 0.75$ and $R^2 = 0.57$, outperforming all other single and combination schemes. Models dominated by visible-band indices (e.g., CIVE, PRI) showed consistently low predictive capacity, whereas those integrating both NIR and visible components achieved higher accuracy. This study confirms that PCM-based redundancy analysis provides an effective framework for guiding VI selection. In particular, combinations with low redundancy and negative correlations were shown to minimize spectral overlap while retaining strong association with AGB, thereby enhancing estimation accuracy. These findings highlight the importance of redundancy-aware selection in developing robust biomass estimation models from high-resolution satellite data.*

Keywords: *Aboveground Biomass, Vegetation Indices, Pearson Correlation Matrix, Multivariate Regression, Correlation Analysis*

Introduction

One approach to reducing atmospheric CO_2 levels and mitigating the effects of climate change is to leverage the role of forests as major carbon sinks (Mina et al., 2017; Poudel et al., 2023). Over the past several decades, remote sensing methods and approaches have been widely used to estimate aboveground biomass (AGB) at local, regional, and even global scales (Allen et al.,

2019; Subedi and Zurqani, 2024). Accurate biomass and carbon-stock calculations require information on vegetation height and density, which can be derived from multispectral or hyperspectral imagery (Tilly et al., 2015). Remote sensing imagery provides accurate, wide-area, and well-calibrated data for this purpose (Kamal et al., 2015; Puliti et al., 2021; Subedi & Zurqani, 2024; Zhang et al., 2023).

Recent advances in remote sensing technology now allow higher spatial and temporal data acquisition (Avitabile et al., 2016). Successful satellite-based mapping of forest carbon requires careful selection of imagery to achieve acceptable mapping accuracy (Madundo et al., 2023). High-resolution data such as PlanetScope SuperDove, with a spatial resolution of about 3 m and near-daily acquisition frequency, makes monitoring forest carbon stocks more feasible (Matiza et al., 2024; Zhao et al., 2022). The choice of analytical methods and the integration of spatial datasets during processing can also improve the quality of AGB maps (De Alban et al., 2021; Pickstone et al., 2025; Shinde & Durbha, 2023).

Despite these advantages for efficiently mapping large areas, several challenges remain in tropical forest carbon estimation using remote sensing (Bronisz et al., 2021). The high diversity of tree species creates considerable spectral variability, complicating species-level mapping (Ferreira et al., 2015; Phillips et al., 2019). Strong heterogeneity related to successional stages, such as primary and secondary forests, further hampers differentiation and calls for more sophisticated approaches (Bispo et al., 2019). In such heterogeneous environments, combining multiple methods or multi-source datasets can enhance aboveground carbon (AGC) modeling accuracy, though the inherent complexity of tropical forests still presents many challenges (Guitet et al., 2015; Muhe & Argaw, 2022; Nesha et al., 2020; Salazar Villegas et al., 2023; Xie et al., 2025). Another limitation is spectral saturation in areas of very high biomass, which can restrict the effective representation of vegetation signals (Z. Chen et al., 2025).

Problem Statement

The use of single vegetation indices often suffers from spectral redundancy, which can reduce the accuracy of aboveground biomass (AGB) estimation (Gu et al., 2013; Tian et al., 2025). Vegetation indices are highly sensitive to soil and atmospheric reflectance factors, such as aerosols (Xu et al., 2022). For example, applying the Normalized Difference Vegetation Index (NDVI) in areas with high biomass saturation frequently yields less accurate biomass estimates (Hu et al., 2025).

By contrast, combining multiple indices is far more effective in minimizing error than relying on a single index (Xu et al., 2022). Integrating several vegetation-index methods can reduce

disturbances caused by soil and geomorphological factors, thereby producing more reliable AGB outputs (Yue et al., 2025). Several studies have reported that combining indices such as NDVI for general vegetation signals, SAVI for soil adjustment, and EVI for atmospheric correction improves the accuracy of AGB estimates compared to using a single index (Qiu et al., 2024; Tam et al., 2025).

Objective

PlanetScope imagery has been recognized as a highly precise optical data source for estimating aboveground biomass (AGB), especially when paired with advanced modeling approaches (Madundo et al., 2023). Various vegetation indices (VIs), such as NDVI, SAVI, and EVI, have proven effective in quantifying biomass, with SAVI often demonstrating the strongest predictive capability for green vegetation; however, the use of multiple indices requires careful consideration of their inter-index correlations to avoid redundant spectral information (Ogungbuyi et al., 2025). Equally important, the integration of field-measured data provides essential validation, ensuring that AGB models remain reliable and accurately reflect on-the-ground forest conditions (Kieu Manh Huong et al., 2023; Madundo et al., 2023).

The Pearson Correlation Matrix (PCM), which consists of Pearson Correlation Coefficients (PCCs) for all pairwise comparisons, is widely used in remote sensing to identify redundancy among spectral indices and improve model accuracy (Viljanen et al., 2018). By providing a complete overview of inter-index correlations, PCM enables adaptive band selection and highlights indices that carry distinct, non-overlapping information (Y.-L. Chen et al., 2020; Kahaer et al., 2020). For example, researchers have applied PCC to examine the relationship between land surface temperature and vegetation density, revealing a clear negative correlation (Nisaa' & Sari, 2025).

In this study, PCM was applied to evaluate the relationships among VIs and to identify which indices contribute most effectively to AGB prediction. Beyond detecting redundancy, PCM also provided a quantitative basis for selecting both single indices and index combinations, guiding regression modeling with reduced overlap in spectral information (Azman et al., 2006; Díaz-Vallejo et al., 2024; Jayaweera & Aziz, 2018; Sathasivam et al., 2022; Wang et al., 2024). While PCM primarily captures linear relationships and may not reflect complex multi-variable interactions, it remains a robust first step for identifying key predictors; complementary approaches such as distance correlation or other advanced measures can be used to further explore potential non-linear patterns (Fu et al., 2025; Ratnasingam & Muñoz-Lopez, 2023).

Methodology

The study was conducted in Wanagama Forest, a research and educational forest managed by Universitas Gadjah Mada in Gunungkidul Regency, Yogyakarta, Indonesia. Covering roughly 622.25 ha, Wanagama is a mixed tropical dry forest with varied topography from gentle hills to steep limestone formations and is characterized by 17 functional vegetation groupings and 14 species variations (Universitas Gadjah Mada, 2025). The area experiences a monsoonal climate with distinct wet and dry seasons, supporting diverse stands such as teak (*Tectona grandis*), acacia (*Acacia auriculiformis*), and other native hardwoods. This structural and floristic diversity makes Wanagama an excellent site for high-resolution remote-sensing studies of aboveground biomass.

The primary dataset for this study consists of PlanetScope Super Dove imagery, which provides 3 m spatial resolution and enables detailed mapping of forest heterogeneity and above-ground biomass (AGB) variation (Matiza et al., 2024; Purnamasari et al., 2021). When analyzed with appropriate methods, these data enhance gradient detection and are effective for estimating forest biomass and related carbon dynamics (Csillik & Asner, 2020). In addition, the high spectral resolution supports the application of diverse vegetation-index (VI) algorithms, an essential step for accurate AGB estimation (Matiza et al., 2024; Purnamasari et al., 2021). The overall workflow for data processing and biomass modeling is illustrated in Figure 1.
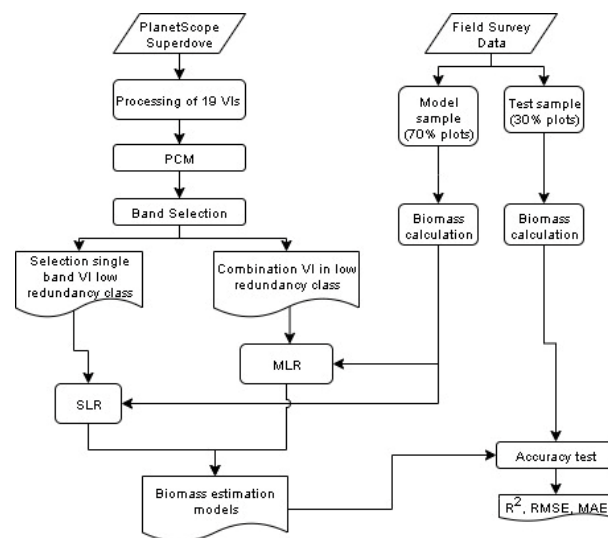

Figure 1: Flowchart of Methodology

Figure 1 summarizes the methodological framework of this study. PlanetScope imagery was processed to generate 18 vegetation indices (VIs), which were then subjected to PCM analysis for band selection. Based on the selected low-redundancy VIs, modeling was carried out using two approaches: simple linear regression (SLR) for single indices and multiple linear

regression (MLR) for multi-index combinations. Field data were divided into 70% for training and 30% for testing to support biomass calculation and model validation. Model performance was evaluated using the statistical indicators coefficient of determination (R^2), root mean square error (RMSE), and mean absolute error (MAE).

a. Vegetation Indices Selection

Selecting appropriate vegetation indices (VIs) is a crucial step in remote sensing analysis for vegetation monitoring, carbon estimation, and land cover classification. With a wide range of indices available, it is essential to reduce redundancy and retain only those with high sensitivity to vegetation structure or physiology, while minimizing inter-correlation. Therefore, the vegetation indices can be systematically grouped based on their spectral characteristics and functional roles, as summarized in the Table 1.

Table 1: List of Vegetation Indices by Category (Processed by the authors)

Category	Indices
General Vegetation	Normalized Difference Vegetation Index (NDVI), Green Leaf Index (GLI), Normalized Green Red Difference Index (NGRDI), Modified Green Red Vegetation Index (MGRVI)
Soil	Soil Adjusted Vegetation Index (SAVI), Green Normalized Difference Vegetation Index (GNDVI)
Atmospheric	Photochemical Reflectance Index (PRI), Enhance Vegetation Index (EVI)
Specific Conditions	Normalized Difference Red Edge (NDRE), Normalized Difference Yellow Vegetation Index (NDYVI), Color Index of Vegetation Extraction (CIVE), Renormalized Difference Vegetation Index (RDVI)
Water	Vogelmann Red Edge Index 1 (VREI1), Vogelmann Red Edge Index 2 (VREI2), Difference Vegetation Index (DVI),
Composite	Blue Green Ratio (BGR), Red Green Ratio (RGR), Red Green Blue Vegetation Index (RGBVI)

There are many variations of vegetation index (VI) algorithms, each designed to emphasize or suppress specific spectral characteristics. The most widely used VI is the Normalized Difference Vegetation Index (NDVI) NDVI (Rouse et al., 1974; Tucker, 1979; Vélez et al., 2023), but for general vegetation conditions other algorithms such as GLI, NGRDI, or MGRVI can also be applied (Bendig et al., 2015; Hunt et al., 2005; Louhaichi et al., 2001). When the goal is to reduce atmospheric effects such as aerosols, indices like PRI or EVI are appropriate

choices (Gamon et al., 1997; Huete et al., 2002; Vélez et al., 2023). To account for vegetation water content or stress, VREI1, VREI2, or DVI can be used (Roujean & Breon, 1995; Vogelmann et al., 1993). In areas where soil reflectance is significant, such as sparsely vegetated regions, SAVI or GNDVI are suitable alternatives (Arshad et al., 2023; Tiruneh et al., 2022; Zhen et al., 2021).Other indices, including BGR, RGR, and RGBVI, employ composite or band ratio techniques (Bendig et al., 2015; C. Chen et al., 2024; Gamon & Surfus, 1999; Sellaro et al., 2010). For applications targeting specific vegetation types, indices such as NDRE, NDYVI, CIVE, or RDVI may also be considered (Boiarskii, 2019; C. Chen et al., 2024; Kataoka et al., 2003; Roujean & Breon, 1995; Wei et al., 2024).

b. Pearson Correlation Matrix (PCM)

PCM is a statistical tool used to examine the linear relationships among multiple variables simultaneously. Each cell in the matrix contains the PCC, ranging from –1 to +1, which indicates both the strength and direction of the association between two indices, and was applied in this study to systematically identify redundant indices and prioritize those with low correlation values for subsequent modeling (Pan, 2022; Sathasivam et al., 2022). In remote sensing applications—such as aboveground biomass estimation—PCM is especially valuable for screening spectral indices or other predictors before modeling (Eckert, 2012; Sathasivam et al., 2022). By examining pairs of variables with strong positive or negative PCM, researchers can pinpoint redundant inputs and focus on spectral indices that carry distinct, non-overlapping information (Jia et al., 2022; Tang & Xu, 2017).

PCC quantifies the strength and direction of a linear relationship between two continuous variables and is expressed as:

$$r = \frac{\sum(x_i - \bar{x})(y_i - \bar{y})}{\sqrt{\sum(x_i - \bar{x})^2}\sqrt{\sum(y_i - \bar{y})^2}}$$

where x_i and y_i are paired observations and $\bar{x}$; $\bar{y}$ are their means. Values of r range from –1 (perfect negative) to +1 (perfect positive), with 0 indicating no linear association (Pearson, 1895).

When arranged into a PCM, these coefficients offer a clear overview of how variables relate to one another, helping researchers detect overlapping spectral indices and choose features that provide distinct, non-redundant information for remote sensing studies (Eckert, 2012). Because of its simple calculation and ease of interpretation, PCM is commonly adopted as an initial step in selecting key variables for aboveground biomass and carbon stock assessments.

The PCM was calculated to evaluate the pairwise relationships among all vegetation indices (VIs). Correlation values were grouped into redundancy classes based on their magnitude: low redundancy (+0 to +0.5 and –0.5 to 0), moderate redundancy (+0.5 to +0.7 and –0.7 to –0.5), high redundancy (+0.7 to +0.9 and –0.9 to –0.7), and strong redundancy or inverse (± 1). Priority was assigned to VIs within the low redundancy class, as these contain the least overlapping spectral information. From this class, indices that appeared as candidates were considered either as single predictors or as part of multi-index combinations. The selection of combinations followed two steps: (i) grouping indices with at least three members connected through low redundancy relationships, and (ii) forming positive and negative pairs of indices within the same low redundancy class. At this stage, the number of single indices and combinations was not predetermined, since it depended on the PCM results.

c. Model Development

To represent and evaluate the relationships identified through the PCManalysis, two types of regression modeling were applied. Simple Linear Regression (SLR) was used for each single VI model, while Multiple Linear Regression (MLR) was applied to the two multi-VI combinations. In these models, the VI values served as the independent variables (x), and the field-measured aboveground biomass data from forest surveys were used as the dependent variable (y).

d. Field Survey and Aboveground Biomass Estimation

The sampling technique employed was random sampling distributed across the entire forest area. A total of 137 samples were collected for model development. Field measurements included diameter at breast height (DBH), total height, and wood density were used to calculate aboveground biomass and its corresponding carbon content through standard allometric equations. Aboveground biomass (AGB) for each tree was calculated using the allometric equation proposed by Chave et al., (2014):

$$AGB_{tree} = 0.0673 * (\rho * DBH^2 * H)^{0.976}$$

where ρ is wood density (g cm⁻³), DBH is diameter at breast height (cm), and H is tree height (m).

Total plot-level AGB was obtained by summing the individual tree values and then converted to an areal basis following IPCC (2006) guidelines:

$$AGB(kg/m^2) = \frac{\sum AGB_{tree}}{A}$$

with A representing the plot area in square meters.

e. Regression Formulas

The modeling employed two regression approaches to estimate AGB from the selected vegetation indices. For each single-index scenario, Simple Linear Regression (SLR) was applied using the equation :

$$y = a + bx$$

where y represents field-measured AGB (ton ha^{-1}), x is the value of the vegetation index, and a and b are the intercept and slope coefficients estimated from the data. For the multi-index combinations, Multiple Linear Regression (MLR) was used with the general form :

$$y = a + b_1 x_1 + b_2 x_2 + \cdots + b_n x_n$$

where $x_1, x_2, \ldots, x_n$ are the vegetation indices included in the combination.

The resulting models were validated using regression analysis with 63 independent samples from field measurements. Model performance was evaluated using the coefficient of determination (R^2), root mean square error (RMSE), and mean absolute error (MAE).

Result and Discussion

The initial processing stage involved pre-processing PlanetScope SuperDove imagery recorded on August 6, 2025, including the calibration of DN values to surface reflectance (percentage) followed by histogram adjustment. The data were then processed using 18 vegetation index (VI) algorithms, resulting in vegetation index images (Figure 2). Most indices ranged from –1 to 1; however, some indices such as CIVE, RGR, and BGR produced values greater than 1. This occurs because these algorithms either operate without a normalization factor or are not based on ratio formulations. Subsequently, 404 randomly distributed pixel samples were extracted from each VI, forming the basis for PCC and PCM calculations.
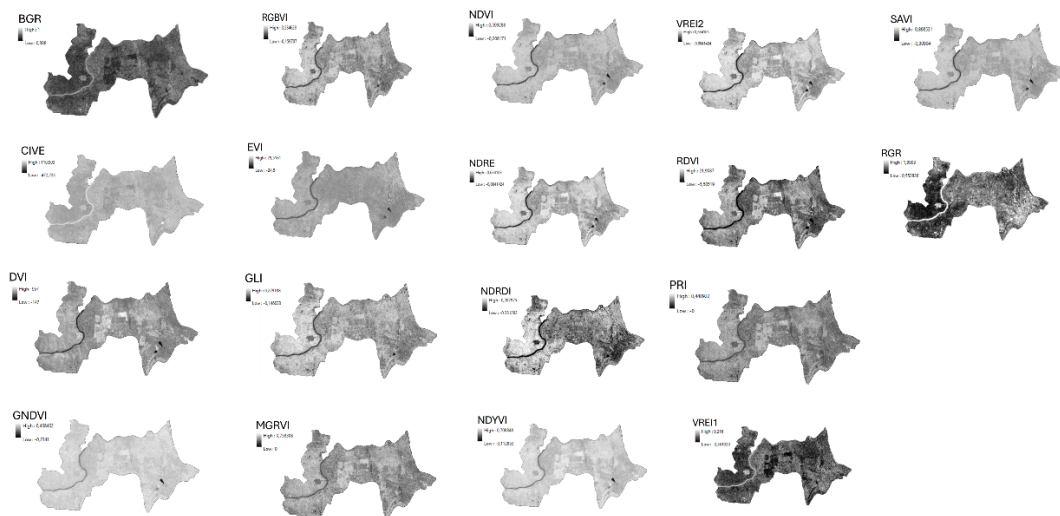

Figure 2: Vegetation Index Image Derived From 18 Algorithms After Pre-processing

Each PCC value (r) ranges from –1.00 to +1.00 and was organized into a PCM to provide a complete view of inter-index correlations. To interpret redundancy, the r values were classified into four categories: low redundancy (–0.5 < r < 0.5), moderate redundancy (0.5 ≤ r < 0.7 or –0.7 < r ≤ –0.5), high redundancy (0.7 ≤ r < 1.0 or –1.0 < r ≤ –0.7), and very strong/strong inverse (r = ±1.0). This matrix served as the foundation for assessing the degree of similarity among the indices.

Based on Table 2, two schemes were applied for selecting vegetation indices. The first scheme grouped indices into single and multi-index combinations without considering the sign of their pairwise correlations, while the second scheme separated the combinations according to positive and negative correlation values. From these procedures, a set of single indices and several index combinations were obtained, as illustrated in Figure 2. In total, sixteen biomass-estimation models were established—covering both single- and multi-index cases—which were then subjected to accuracy evaluation.

Table 2: Pearson Correlation Matrix of 18 Vegetation Indice (Processed by the authors)

	NDVI	EVI	SAVI	GNDVI	NDRE	NDYVI	CIVE	MGRVI	RGBVI	GLI	NGRDI	RGR	BGR	PRI	VREI1	VREI2	DVI	RDVI
NDVI	1.00	0.86	0.88	0.93	0.92	0.96	-0.70	-0.77	0.77	0.77	0.77	-0.78	-0.67	0.65	0.92	0.92	0.78	0.91
EVI	0.86	1.00	1.00	0.84	0.82	0.84	-0.65	-0.63	0.62	0.63	0.63	-0.63	-0.54	0.53	0.79	0.82	0.99	0.99
SAVI	0.88	1.00	1.00	0.87	0.84	0.88	-0.65	-0.62	0.63	0.63	0.62	-0.62	-0.56	0.56	0.80	0.84	0.98	1.00
GNDVI	0.93	0.84	0.87	1.00	0.92	0.96	-0.42	-0.49	0.51	0.51	0.49	-0.50	-0.47	0.46	0.76	0.92	0.78	0.89
NDRE	0.92	0.82	0.84	0.92	1.00	0.90	-0.50	-0.62	0.62	0.62	0.62	-0.62	-0.53	0.53	0.73	1.00	0.75	0.86
NDYVI	0.96	0.84	0.88	0.96	0.90	1.00	-0.63	-0.64	0.70	0.69	0.64	-0.65	-0.70	0.69	0.85	0.90	0.78	0.90
CIVE	-0.70	-0.65	-0.65	-0.42	-0.50	-0.63	1.00	0.90	-0.94	-0.93	-0.90	0.91	0.87	-0.85	-0.81	-0.50	-0.61	-0.67
MGRVI	-0.77	-0.63	-0.62	-0.49	-0.62	-0.64	0.90	1.00	-0.95	-0.98	-1.00	1.00	0.79	-0.78	-0.89	-0.62	-0.55	-0.66
RGBVI	0.77	0.62	0.63	0.51	0.62	0.70	-0.94	-0.95	1.00	1.00	0.95	-0.95	-0.94	0.93	0.87	0.62	0.55	0.66
GLI	0.77	0.63	0.63	0.51	0.62	0.69	-0.93	-0.98	1.00	1.00	0.98	-0.97	-0.90	0.90	0.88	0.62	0.56	0.66
NGRDI	0.77	0.63	0.62	0.49	0.62	0.64	-0.90	-1.00	0.95	0.98	1.00	-1.00	-0.79	0.78	0.89	0.62	0.55	0.66
RGR	-0.78	-0.63	-0.62	-0.50	-0.62	-0.65	0.91	1.00	-0.95	-0.97	-1.00	1.00	0.79	-0.78	-0.89	-0.62	-0.54	-0.66
BGR	-0.67	-0.54	-0.56	-0.47	-0.53	-0.70	0.87	0.79	-0.94	-0.90	-0.79	0.79	1.00	-1.00	-0.75	-0.53	-0.50	-0.59
PRI	0.65	0.53	0.56	0.46	0.53	0.69	-0.85	-0.78	0.93	0.90	0.78	-0.78	-1.00	1.00	0.74	0.53	0.49	0.58
VREI1	0.92	0.79	0.80	0.76	0.73	0.85	-0.81	-0.89	0.87	0.88	0.89	-0.89	-0.75	0.74	1.00	0.73	0.70	0.83
VREI2	0.92	0.82	0.84	0.92	1.00	0.90	-0.50	-0.62	0.62	0.62	0.62	-0.62	-0.53	0.53	0.73	1.00	0.75	0.86
DVI	0.78	0.99	0.98	0.78	0.75	0.78	-0.61	-0.55	0.55	0.56	0.55	-0.54	-0.50	0.49	0.70	0.75	1.00	0.97
RDVI	0.91	0.99	1.00	0.89	0.86	0.90	-0.67	-0.66	0.66	0.66	0.66	-0.66	-0.59	0.58	0.83	0.86	0.97	1.00

- Low redundancy (-)
- Low redundancy (+)
- Moderate redundancy
- High redundancy
- Very strong correlation or strong inverse

For the multi-index combinations, two selection schemes were applied. In the first scheme, indices were grouped directly from the PCM by prioritizing those that maintained low redundancy relationships, resulting in four candidate combinations (Comb 1–4). In the second scheme, the same groups were further refined by separating positive and negative correlation

values, which produced additional combinations. This two-step procedure ensured that the selected multi-index models represented both general low-redundancy groups and polarity-specific relationships, consistent with the flow illustrated in Table 3.

Table 3: Summary of Vegetation Index (VI) Candidates and Multi-Index Combinations Derived from PCM Analysis

Single Index Candidates	Mixed Combinations (No ± separation)	Separated Combinations (± based)
GNDVI CIVE MGRVI NGRDI RGR BGR PRI DVI	Comb 1: GNDVI – CIVE – MGRVI – NGRDI – RGR – BGR – PRI	Comb 1(+): GNDVI – NGRDI – PRI
	Comb 2: BGR – GNDVI – DVI	Comb 2(+): PRI – GNDVI – DVI
	Comb 3: PRI – GNDVI – DVI	Comb 1(–): GNDVI – CIVE – MGRVI – RGR – BGR
	Comb 4: DVI – BGR – PRI	Comb 2(–): BGR – GNDVI – DVI

The single-band indices were processed using SLR with AGB data obtained from field measurements and sample-based calculations. The resulting SLR plots display the distribution of field samples against the pixel values of each single VI, with the coefficient of determination varying noticeably across indices. However, further analysis is required by comparing the correlation strength and the predictive performance of the estimated AGB values, as illustrated in Figure *3*.
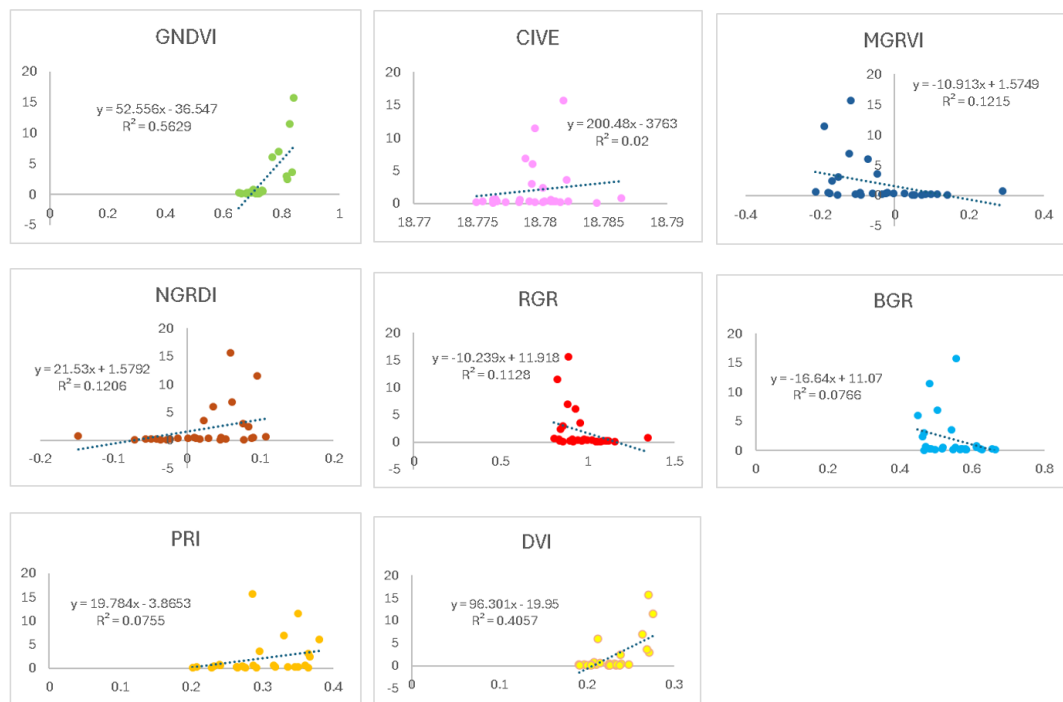

Figure 3: Simple Linear Regression (SLR) of AGB with Selected Single VI

Among the single indices tested, GNDVI ($R^2 = 0.5629$) and DVI ($R^2 = 0.4057$) emerged as the best-performing predictors for AGB, largely because they incorporate the near-infrared (NIR) band in combination with green or red reflectance. The strong response of NIR to vegetation structure allows these indices to capture canopy density and chlorophyll content more effectively, leading to higher predictive accuracy. In contrast, indices such as CIVE ($R^2 = 0.02$), BGR ($R^2 = 0.0766$), and PRI ($R^2 = 0.0755$) showed poor performance because they are derived exclusively from visible bands (blue, green, or red). These bands are more sensitive to soil background, shadow, and illumination effects, reducing their capacity to reflect biomass variation. For instance, CIVE and BGR, which rely heavily on visible reflectance, often saturate in dense canopy conditions and underestimate biomass in high-biomass plots, while PRI is strongly affected by pigment variation and provides limited structural information. Conversely, indices dominated by NIR contrast, such as DVI and GNDVI, benefit from the sharp spectral separation between vegetation absorption in red/green and strong reflection in NIR, making them more responsive to biomass gradients.

Table 4: Summary of regression performance (R and R^2) for multi-index models using Multiple Linear Regression (MLR)

Regression Statistics	Com1	Com2	Com3	Com4	Com1+	Com2+	Com1-	Com2-
Multiple R	0.82	0.69	0.56	0.74	0.64	0.56	0.82	0.69
R Square	0.68	0.48	0.31	0.54	0.4	0.31	0.67	0.48

Table 4 presents the summary results of multi-index modeling using MLR. Among the tested combinations, Com1 ($R^2 = 0.68$) and Com1– ($R^2 = 0.67$) achieved the highest performance, indicating that these combinations capture complementary spectral information that effectively reduces unexplained variance in AGB estimation. Both sets include indices dominated by NIR and visible bands (e.g., GNDVI, BGR, PRI, CIVE), where the NIR component enhances sensitivity to canopy structure, while the visible bands contribute information on pigment variation and soil–vegetation contrast. The integration of these complementary spectral features likely explains their superior predictive capacity.

In contrast, Com3 and Com2+ ($R^2 = 0.31$) yielded the weakest performance, suggesting that the indices included in these groups may share redundant spectral information, limiting their contribution to the overall model. Moderate results were observed for Com4 ($R^2 = 0.54$) and Com2 ($R^2 = 0.48$), reflecting partial complementarity but also some redundancy effects.

These findings support the hypothesis that redundancy plays a critical role in multi-index modeling. When input indices are highly correlated, their overlapping spectral responses fail

to add new information, resulting in lower model accuracy. Conversely, when indices with distinct yet complementary spectral patterns are combined, redundancy is minimized and the model benefits from a more diverse representation of vegetation properties, thereby improving biomass estimation. This highlights the importance of careful index selection to balance redundancy and complementarity in multi-index biomass models.

To better illustrate the spatial outcomes, Figure 4 present the distribution of aboveground biomass derived from the sixteen developed models (eight single-index and eight multi-index). In both cases, biomass values are expressed as ton/ha per 3 × 3 m pixel, with negative values representing non-vegetated areas (e.g., built-up zones or water bodies). The maps highlight the variation in biomass estimation across Wanagama, where multi-index models generally provide smoother and more consistent patterns compared to single-index models.
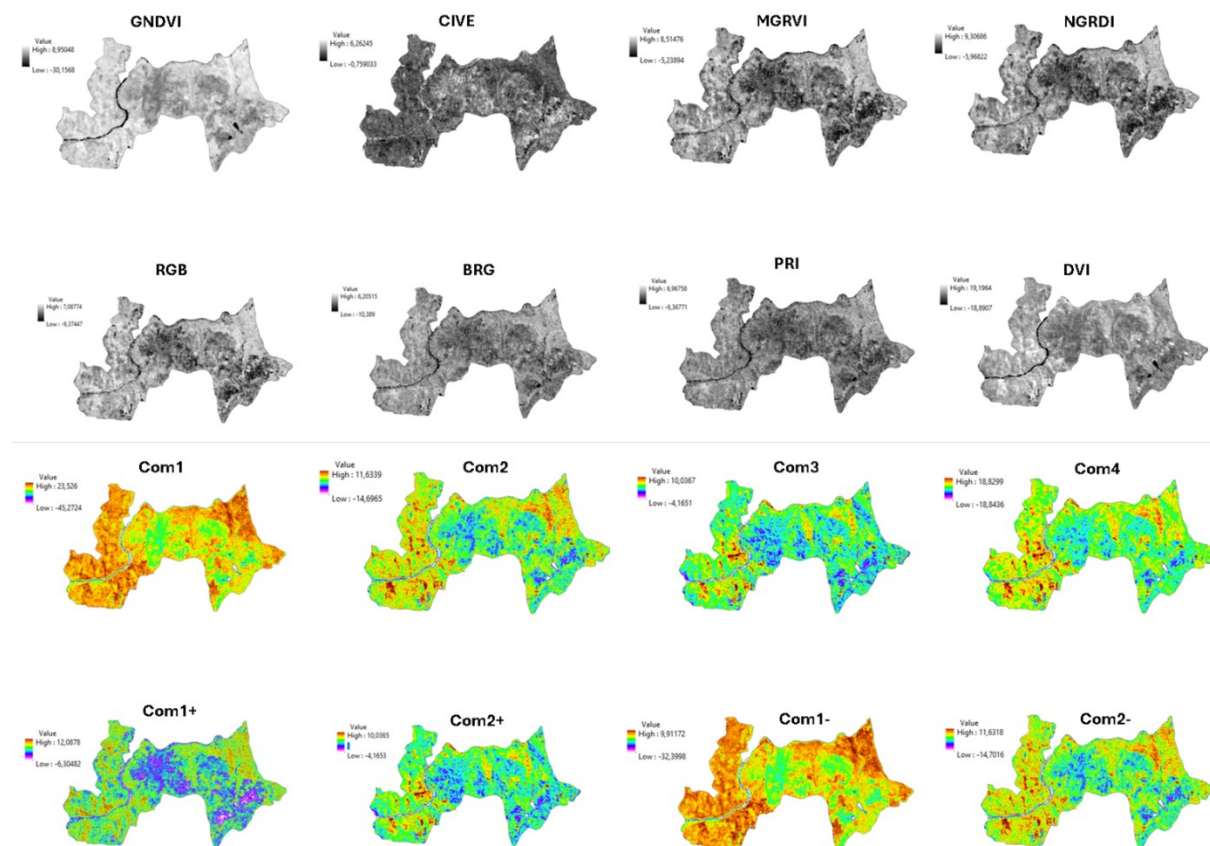

Figure 4: Spatial distribution of aboveground biomass (AGB) from single-index models (greyscale) and multi-index models (color), where negative values represent non-vegetated areas

Finally, the quantitative performance of these sixteen models was evaluated against field-measured AGB in the study area. Model validation was carried out using 30% of the samples, corresponding to 63 field plots. The metrics assessed were correlation coefficient (R),

coefficient of determination (R²), root mean square error (RMSE), and mean absolute error (MAE), with the results summarized in Table 5.

Table 5: Performance Of VI-Based Models (Single and Multi-Index) for AGB Estimation with Total Estimated Biomass

	Total Ha (Estimation)	R	R2	RMSE	MAE
GNDVI	1,929.2	0.69	0.48	3.32	2.49
CIVE	1,195.7	0.14	0.02	1.73	1.66
MGRVI	1,424.4	0.40	0.16	2.28	2.03
NGRDI	1,426.8	0.40	0.16	2.28	2.03
RGR	1,399.5	0.39	0.15	2.23	2.03
BGR	1,228.7	0.39	0.15	2.21	2.03
PRI	1,225.7	0.38	0.15	2.21	2.02
DVI	2,217.2	0.38	0.14	3.40	2.55
Comb1	2,060.2	0.66	0.44	3.51	2.45
Comb2	1,742.9	0.54	0.29	3.00	2.50
Comb3	1,671.1	0.05	0.00	2.34	2.09
Comb4	2,194.5	0.39	0.15	3.40	2.60
Com1+	1,737.9	0.48	0.23	3.24	2.29
Com2+	1,671.0	0.35	0.12	3.49	2.40
Com1-	1,928.9	0.75	0.57	2.42	1.78
Com2-	1,741.6	0.57	0.33	3.02	2.08

By contrast, models dominated by indices with higher redundancy or confined to visible bands only (e.g., CIVE or PRI) showed weak predictive capability, as the spectral information overlapped or failed to represent canopy structural variability. These findings confirm the role of redundancy in shaping model performance: when redundancy is minimized—especially through negative correlations—multi-index combinations can significantly improve biomass estimation accuracy. In addition, the estimation values (Total Ha) demonstrate that models with stronger correlation, such as GNDVI and particularly Comb1-, not only achieved higher R and R² but also produced more consistent biomass estimates relative to the expected range of forest productivity. Importantly, the best-performing model (Comb1-) incorporated indices such as CIVE and RGR, which individually showed weak predictive capacity, but when integrated with GNDVI, MGRVI, and BGR, their complementary spectral information helped reduce redundancy and capture canopy structure more effectively. This highlights that indices with

limited standalone performance can still play a critical role in multi-index frameworks, ultimately improving the robustness of AGB estimation.

The comparison between the regression statistics obtained from model development and the independent accuracy test reveals several key patterns (Figure 5). First, Com1– consistently outperformed other models, with high values of R and R^2 both in the model stage and the accuracy test ($R^2 = 0.67$ in the model, $R^2 = 0.57$ in validation). This consistency indicates that the negative redundancy within its index composition provides complementary spectral information that generalizes well to unseen samples. Similarly, GNDVI (single index) and Com1 (multi-index) also maintained relatively strong performance across both stages, confirming the advantage of incorporating NIR-sensitive indices in biomass prediction.
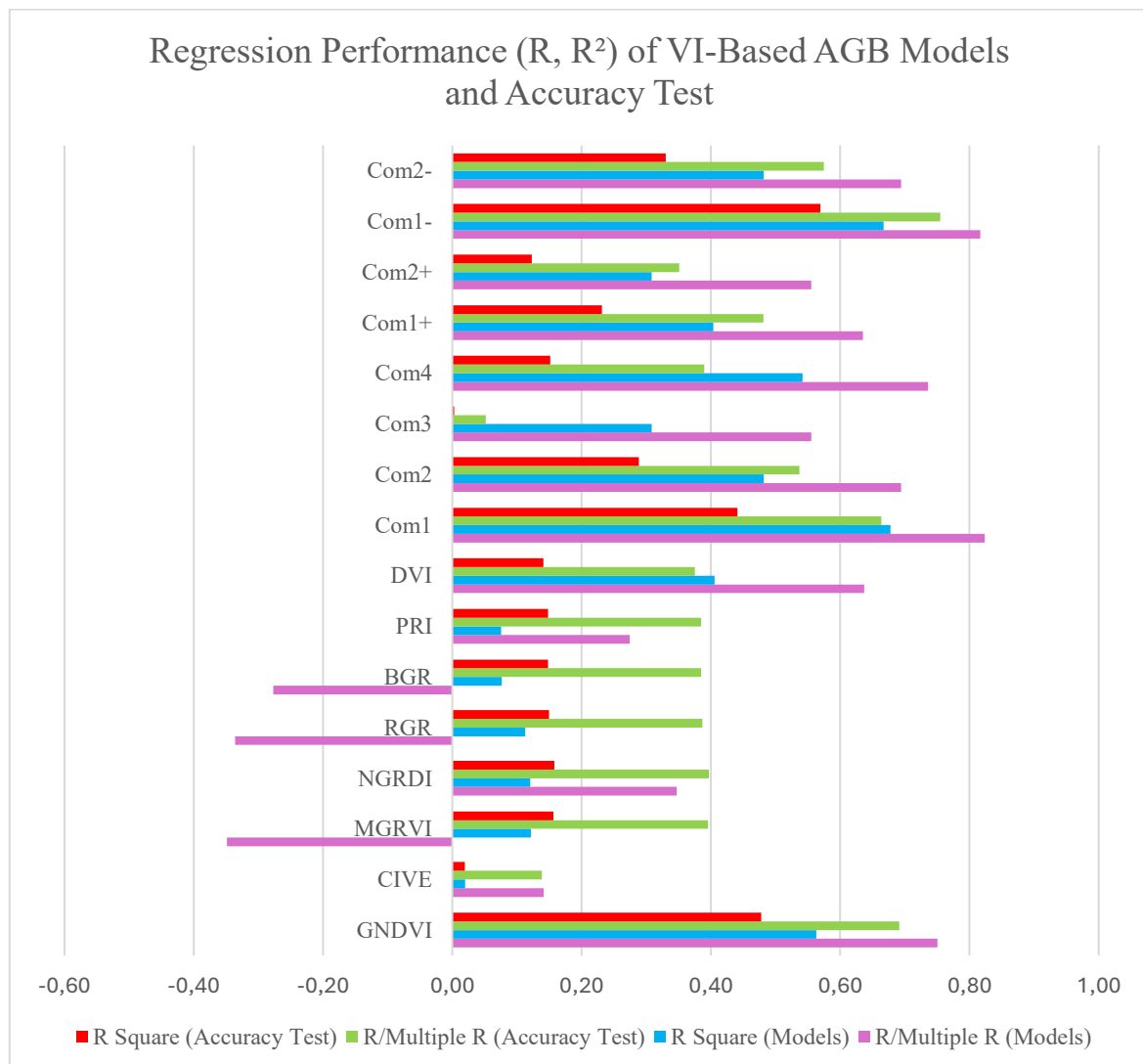

Figure 5: Comparison of Regression Performance (R, R^2) Between Model Calibration and Accuracy Test for VI-Based AGB Estimation

On the other hand, models such as Com3, CIVE, and PRI showed low R and R² values in both training and validation, highlighting their limited predictive capacity. These indices rely mainly on visible bands, which are more influenced by soil, illumination, and canopy background effects, leading to unstable estimation and weak transferability. Interestingly, some models (e.g., DVI and Com2) exhibited a moderate decline from model fit to validation results, suggesting partial overfitting or redundancy among the combined indices.
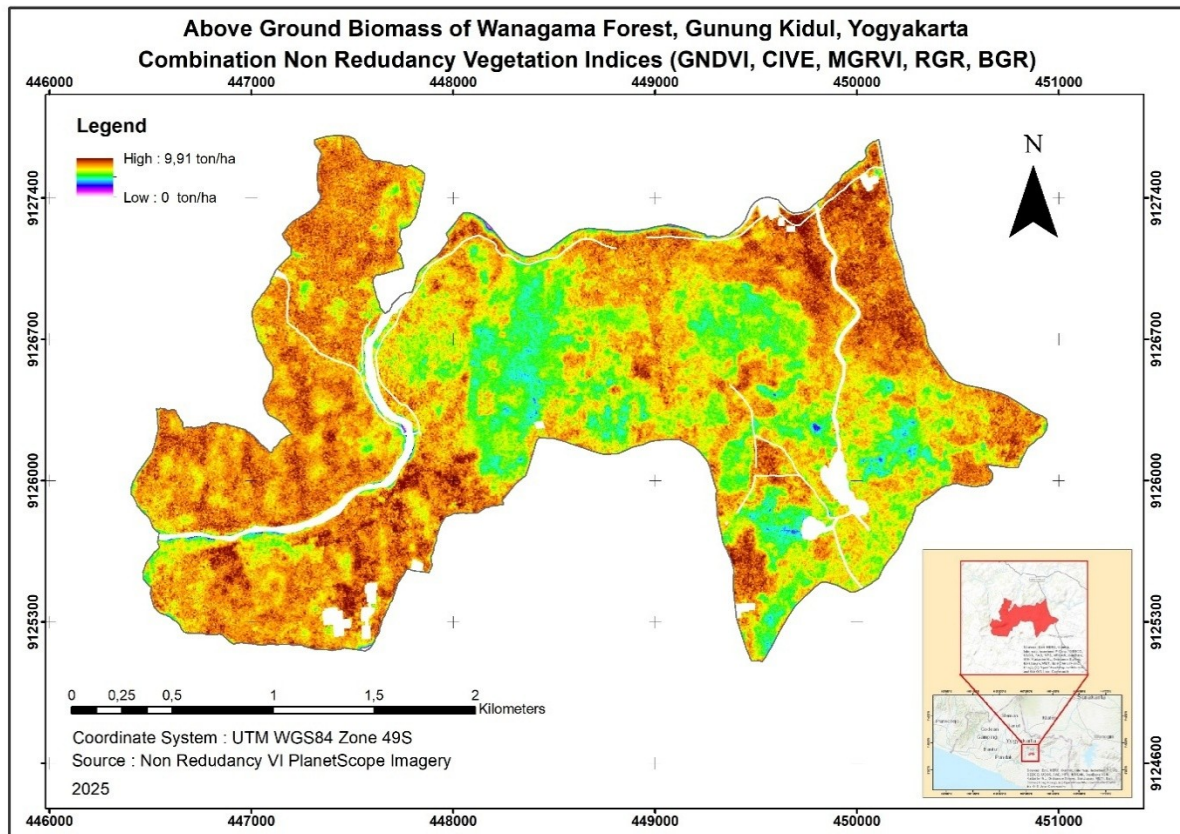

Figure 6: Spatial distribution of Aboveground Biomass (AGB) in Wanagama Forest, Gunung Kidul, Yogyakarta, estimated using the best-performing model (Com1-) based on a non-redundant combination of vegetation indices (GNDVI, CIVE, MGRVI, RGR, and BGR).

Overall, the comparison indicates that models integrating indices with low or negative redundancy tend to preserve accuracy from model calibration to validation, while those dominated by visible-band redundancy are prone to loss of performance. This reinforces the importance of carefully balancing index complementarity and redundancy in order to achieve robust biomass estimation models. As illustrated in Figure 6, the spatial distribution produced by the Com1- model demonstrates how integrating both strong (e.g., GNDVI) and weaker indices (e.g., CIVE and BGR) can yield a more coherent representation of biomass variation. Areas with higher AGB are consistently captured in the northern and central parts of Wanagama, while lower values correspond to riparian zones and degraded patches, confirming

that multi-index combinations not only improve statistical accuracy but also enhance the spatial realism of biomass estimation maps.

Conclusion

The evaluation of vegetation indices (VIs) for aboveground biomass (AGB) estimation demonstrates that each VI carries distinct spectral characteristics, reflecting different aspects of canopy properties. Indices dominated by the near-infrared (NIR) band, such as GNDVI and DVI, showed stronger correlations with AGB due to their sensitivity to vegetation structure and density, whereas indices derived primarily from visible bands (e.g., CIVE, BGR, PRI) exhibited weaker performance as they are more affected by soil background, illumination, and pigment variability. These results underline the need for careful consideration of the spectral properties emphasized or minimized by each VI when selecting predictors for biomass modeling.

The use of the PCM proved effective as a quantitative approach for guiding index selection. By classifying indices into redundancy groups, PCM allowed systematic identification of candidate indices with low overlap in spectral information, which could then be tested both individually and in combination. This procedure facilitated the development of multi-index models through multiple linear regression (MLR), where complementary spectral inputs improved the capacity to explain variability in field-measured AGB.

A key finding is the role of low redundancy and negative correlation in enhancing model accuracy. Multi-index models that incorporated indices with distinct and negatively correlated spectral patterns (e.g., Com1−) consistently yielded higher R and R^2 values while minimizing RMSE and MAE. This suggests that reducing information overlap while maintaining strong correlation with biomass provides the most effective strategy for estimation. In practical terms, the study highlights that biomass modeling should not rely solely on individual indices, but rather on combinations carefully selected through redundancy analysis to achieve optimal predictive accuracy.

References

Arshad, S., Kazmi, J. H., Javed, M. G., & Mohammed, S. (2023). Applicability of machine learning techniques in predicting wheat yield based on remote sensing and climate data in Pakistan, South Asia. *European Journal of Agronomy*, *147*, 126837–126837. https://doi.org/10.1016/j.eja.2023.126837

Avitabile, V., Herold, M., Heuvelink, G. B. M., Lewis, S. L., Phillips, O. L., Asner, G. P., Armston, J., Ashton, P. S., Banin, L., & Bayol, N. (2016). An integrated pan-tropical biomass map using multiple reference datasets. *Global Change Biology*, *22*(4), 1406–1420.

Azman, J., Frković, V., Bilić-Zulle, L., & Petrovecki, M. (2006). Correlation and regression. *Acta Medica Croatica : Casopis Hravatske Akademije Medicinskih Znanosti*, *60 Suppl 1*, 81–91. Scopus.

Bendig, J., Yu, K., Aasen, H., Bolten, A., Bennertz, S., Broscheit, J., Gnyp, M. L., & Bareth, G. (2015). Combining UAV-based plant height from crop surface models, visible, and near infrared vegetation indices for biomass monitoring in barley. *International Journal of Applied Earth Observation and Geoinformation*, *39*, 79–87. https://doi.org/10.1016/j.jag.2015.02.012

Bispo, P. D. C., Pardini, M., Papathanassiou, K. P., Kugler, F., Balzter, H., Rains, D., Dos Santos, J. R., Rizaev, I. G., Tansey, K., Dos Santos, M. N., & Spinelli Araujo, L. (2019). Mapping Forest Successional Stages in The Brazilian Amazon Using Forest Heights Derived from TanDEM-X SAR Interferometry. *Remote Sensing of Environment*, *232*, 111194. https://doi.org/10.1016/j.rse.2019.05.013

Boiarskii, B. (2019). Comparison of NDVI and NDRE Indices to Detect Differences in Vegetation and Chlorophyll Content. *JOURNAL OF MECHANICS OF CONTINUA AND MATHEMATICAL SCIENCES*, *1*(4). https://doi.org/10.26782/jmcms.spl.4/2019.11.00003

Bronisz, K., Bijak, S., Wojtan, R., Tomusiak, R., Bronisz, A., Baran, P., & Zasada, M. (2021). Seemingly Unrelated Mixed-Effects Biomass Models for Black Locust in West Poland. *Forests*, *12*(3), 380. https://doi.org/10.3390/f12030380

Chave, J., Réjou-Méchain, M., Búrquez, A., Chidumayo, E., Colgan, M. S., Delitti, W. B. C., Duque, A., Eid, T., Fearnside, P. M., Goodman, R. C., Henry, M., Martínez-Yrízar, A., Mugasha, W. A., Muller-Landau, H. C., Mencuccini, M., Nelson, B. W., Ngomanda, A., Nogueira, E. M., Ortiz-Malavassi, E., … Vieilledent, G. (2014). Improved allometric models to estimate the aboveground biomass of tropical trees. *Global Change Biology*, *20*(10), 3177–3190. https://doi.org/10.1111/gcb.12629

Chen, C., Yuan, X., Gan, S., Luo, W., Bi, R., Li, R., & Gao, S. (2024). A new vegetation index based on UAV for extracting plateau vegetation information. *International Journal of Applied Earth Observation and Geoinformation*, *128*, 103668–103668. https://doi.org/10.1016/j.jag.2024.103668

Chen, Z., Yang, X., Pan, X., Wu, T., Lei, J., Chen, X., Li, Y., & Chen, Y. (2025). Estimating Forest Aboveground Biomass in Tropical Zones by Integrating LiDAR and Sentinel-2B Data. *Sustainability*, *17*(8), 3631. https://doi.org/10.3390/su17083631

Csillik, O., & Asner, G. P. (2020). Near-real time aboveground carbon emissions in Peru. *PLOS ONE*, *15*(11), e0241418. https://doi.org/10.1371/journal.pone.0241418

De Alban, J. D. T., Veridiano, R. K. A., Pang, S. E. H., Estomata, M. T. L., Jamaludin, J., Jaojoco, A. K. M., Parinas, M. T., Reyes, S. R. C., Tumaneng, R. D., & Verma, A. (2021). *Estimating Aboveground Forest Carbon Stocks Using Multi-Sensor Satellite Data and Field Measurements in The Philippines*. 42nd Asian Conference on Remote Sensing, ACRS 2021. Scopus. https://www.scopus.com/inward/record.uri?eid=2-s2.0-85127373559&partnerID=40&md5=afd54066335f417a0534861983a855a9

Díaz-Vallejo, M., Peña-Peniche, A., Mota-Vargas, C., Piña-Torres, J., Valencia-Rodríguez, D., Rangel-Rivera, C. E., Gaviria-Hernández, J., & Rojas-Soto, O. (2024). Analyses of the variable selection using correlation methods: An approach to the importance of statistical inferences in the modelling process. *Ecological Modelling*, *498*, 110893. https://doi.org/10.1016/j.ecolmodel.2024.110893

Eckert, S. (2012). Improved Forest Biomass and Carbon Estimations Using Texture Measures from WorldView-2 Satellite Data. *Remote Sensing*, *4*(4), 810–829. https://doi.org/10.3390/rs4040810

Ferreira, M. P., Zortea, M., Zanotta, D. C., Féret, J. B., Shimabukuro, Y. E., & Souza Filho, C. R. (2015). ON THE USE OF SHORTWAVE INFRARED FOR TREE SPECIES DISCRIMINATION IN TROPICAL SEMIDECIDUOUS FOREST. *The International Archives of the Photogrammetry, Remote Sensing and Spatial Information Sciences*, *XL-3/W3*, 473–476. https://doi.org/10.5194/isprsarchives-XL-3-W3-473-2015

Fu, H., Tang, S., & Zhao, X. (2025). Limitations of Correlation Coefficients in Research on Functional Connectomes and Psychological Processes. *Human Brain Mapping*, *46*(10), e70287. https://doi.org/10.1002/hbm.70287

Gamon, J. A., Serrano, L., & Surfus, J. S. (1997). The photochemical reflectance index: An optical indicator of photosynthetic radiation use efficiency across species, functional types, and nutrient levels. *Oecologia*, *112*(4), 492–501. https://doi.org/10.1007/s004420050337

Gamon, J. A., & Surfus, J. S. (1999). Assessing leaf pigment content and activity with a reflectometer. *New Phytologist*, *143*(1), 105–117. https://doi.org/10.1046/j.1469-8137.1999.00424.x

Gu, Y., Wylie, B. K., Howard, D. M., Phuyal, K. P., & Ji, L. (2013). NDVI saturation adjustment: A new approach for improving cropland performance estimates in the Greater Platte River Basin, USA. *Ecological Indicators*, *30*, 1–6. https://doi.org/10.1016/j.ecolind.2013.01.041

Guitet, S., Hérault, B., Molto, Q., Brunaux, O., & Couteron, P. (2015). Spatial Structure of Above-Ground Biomass Limits Accuracy of Carbon Mapping in Rainforest but Large Scale Forest Inventories Can Help to Overcome. *PLOS ONE*, *10*(9), e0138456. https://doi.org/10.1371/journal.pone.0138456

Hu, J., Du, X., Li, Q., Zhang, Y., Wang, H., Xu, J., Xiao, J., Shen, Y., Dong, Y., Hu, H., Yan, S., & Gong, S. (2025). Aboveground Biomass Estimation of Highland Barley in Qinghai–Tibet Plateau—Exploring the Advantages of Time Series Data and Terrain Effects. *Remote Sensing*, *17*(4), 655. https://doi.org/10.3390/rs17040655

Huete, A., Didan, K., Miura, T., Rodriguez, E. P., Gao, X., & Ferreira, L. G. (2002). Overview of the radiometric and biophysical performance of the MODIS vegetation indices. *Remote Sensing of Environment*, *83*(1–2), 195–213. https://doi.org/10.1016/S0034-4257(02)00096-2

Hunt, E. R., Cavigelli, M., Daughtry, C. S. T., Mcmurtrey, J. E., & Walthall, C. L. (2005). Evaluation of Digital Photography from Model Aircraft for Remote Sensing of Crop Biomass and Nitrogen Status. *Precision Agriculture*, *6*(4), 359–378. https://doi.org/10.1007/s11119-005-2324-5

IPCC. (2006). *Guidelines for National Greenhouse Gas Inventories* (Volume 4: Agriculture, Forestry and Other Land Use). Agriculture.

Jayaweera, C., & Aziz, N. (2018). Reliability of Principal Component Analysis and Pearson Correlation Coefficient, for Application in Artificial Neural Network Model Development, for Water Treatment Plants. *IOP Conference Series: Materials Science and Engineering*, *458*, 012076. https://doi.org/10.1088/1757-899X/458/1/012076

Jia, P., Zhang, J., He, W., Yuan, D., Hu, Y., Zamanian, K., Jia, K., & Zhao, X. (2022). Inversion of Different Cultivated Soil Types' Salinity Using Hyperspectral Data and Machine Learning. *Remote Sensing*, *14*(22), 5639. https://doi.org/10.3390/rs14225639

Kamal, M., Phinn, S., & Johansen, K. (2015). *Object-based approach for multi-scale mangrove composition mapping using multi-resolution image datasets*. *7*(4), 4783. https://doi.org/10.3390/rs70404753

Kataoka, T., Kaneko, T., Okamoto, H., & Hata, S. (2003). *Crop growth estimation system using machine vision*. *2*, b1079–b1083.

Kieu Manh Huong, Rodríguez-Hernández, D. I., & Tuan, N. T. (2023). Mapping the Above-Ground Biomass of Rhizophora apiculata plantation Forests Using PlanetScope Imagery in Thanh Phu Nature Reserve, Vietnam. *Biology Bulletin*, *50*(S3), S450–S461. https://doi.org/10.1134/S1062359023601957

Louhaichi, M., Borman, M. M., & Johnson, D. E. (2001). Spatially Located Platform and Aerial Photography for Documentation of Grazing Impacts on Wheat. *Geocarto International*, *16*(1), 65–70. https://doi.org/10.1080/10106040108542184

Madundo, S. D., Mauya, E. W., & Kilawe, C. J. (2023). Comparison of multi-source remote sensing data for estimating and mapping above-ground biomass in the West Usambara tropical montane forests. *Scientific African*, *21*, e01763. https://doi.org/10.1016/j.sciaf.2023.e01763

Matiza, C., Mutanga, O., Odindi, J., & Mngadi, M. (2024). The Utility of Planetscope Spectral Data in Quantifying Above-ground Carbon Stock in An Urban Reforested Landscape. *Ecological Informatics*, *80*, 102472. https://doi.org/10.1016/j.ecoinf.2024.102472

Mina, M., Bugmann, H., Cordonnier, T., Irauschek, F., Klopcic, M., Pardos, M., & Cailleret, M. (2017). Future ecosystem services from European mountain forests under climate change. *Journal of Applied Ecology*, *54*(2), 389–401. https://doi.org/10.1111/1365-2664.12772

Muhe, S., & Argaw, M. (2022). Estimation of above-ground biomass in tropical afro-montane forest using Sentinel-2 derived indices. *Environmental Systems Research*, *11*(1), 5. https://doi.org/10.1186/s40068-022-00250-y

Nesha, M. K., Hussin, Y. A., Van Leeuwen, L. M., & Sulistioadi, Y. B. (2020). Modeling and mapping aboveground biomass of the restored mangroves using ALOS-2 PALSAR-2 in East Kalimantan, Indonesia. *International Journal of Applied Earth Observation and Geoinformation*, *91*, 102158. https://doi.org/10.1016/j.jag.2020.102158

Nisaa', R. M., & Sari, U. K. (2025). Assessing the Relationship Between Land Surface Temperature and Vegetation Index During Revegetation Activities: A Remote Sensing Study on Berau Regency, East Kalimantan (2015-2021). *Media Konservasi*, *30*(2), 262. https://doi.org/10.29244/medkon.30.2.262

Ogungbuyi, M. G., Guerschman, J., Fischer, A. M., Mohammed, C., Crabbe, R. A., & Harrison, M. T. (2025). Using vegetation indices from nanosatellites for timely prediction of pasture biomass. *Total Environment Advances*, *15*, 200130. https://doi.org/10.1016/j.teadva.2025.200130

Pan, G. (2022). Correlation Coefficient. In B. S. Daya Sagar, Q. Cheng, J. McKinley, & F. Agterberg (Eds.), *Encyclopedia of Mathematical Geosciences* (pp. 1–9). Springer International Publishing. https://doi.org/10.1007/978-3-030-26050-7_69-1

Pearson, K. (1895). VII. Note on regression and inheritance in the case of two parents. *Proceedings of the Royal Society of London*, *58*(347–352), 240–242. https://doi.org/10.1098/rspl.1895.0041

Phillips, O. L., Sullivan, M. J. P., Baker, T. R., Monteagudo Mendoza, A., Vargas, P. N., & Vásquez, R. (2019). Species Matter: Wood Density Influences Tropical Forest Biomass at Multiple Scales. *Surveys in Geophysics*, *40*(4), 913–935. https://doi.org/10.1007/s10712-019-09540-0

Pickstone, B. J., Graham, H. A., & Cunliffe, A. M. (2025). Estimating Canopy Height in Tropical Forests: Integrating Airborne LiDAR and Multi-spectral Optical Data with Machine Learning. *Sustainable Environment*, *11*(1), 2469406. https://doi.org/10.1080/27658511.2025.2469406

Poudel, A., Shrestha, H. L., Mahat, N., Sharma, G., Aryal, S., Kalakheti, R., & Lamsal, B. (2023). Modeling and Mapping of Aboveground Biomass and Carbon Stock Using

Sentinel-2 Imagery in Chure Region, Nepal. *International Journal of Forestry Research*, *2023*, 1–12. https://doi.org/10.1155/2023/5553957

Puliti, S., Breidenbach, J., Schumacher, J., Hauglin, M., Klingenberg, T. F., & Astrup, R. (2021). Above-ground biomass change estimation using national forest inventory data with Sentinel-2 and Landsat. *Remote Sensing of Environment*, *265*, 112644–112644. https://doi.org/10.1016/j.rse.2021.112644

Purnamasari, E., Kamal, M., & Wicaksono, P. (2021). Comparison of vegetation indices for estimating above-ground mangrove carbon stocks using PlanetScope image. *Regional Studies in Marine Science*, *44*, 101730.

Qiu, B., Li, S., Cao, J., Zhang, J., Yang, K., Luo, K., Huang, K., & Jiang, X. (2024). Uncertainty Analysis of Forest Aboveground Carbon Stock Estimation Combining Sentinel-1 and Sentinel-2 Images. *Forests*, *15*(12), 2134. https://doi.org/10.3390/f15122134

Ratnasingam, S., & Muñoz-Lopez, J. (2023). Distance Correlation-Based Feature Selection in Random Forest. *Entropy*, *25*(9), 1250. https://doi.org/10.3390/e25091250

Roujean, J.-L., & Breon, F.-M. (1995). Estimating PAR absorbed by vegetation from bidirectional reflectance measurements. *Remote Sensing of Environment*, *51*(3), 375–384. https://doi.org/10.1016/0034-4257(94)00114-3

Rouse, J. W., Haas, R. H., Schell, J. A., & Deering, D. W. (1974). Monitoring vegetation systems in the Great Plains with ERTS. *NASASpecialPublication*, 309–317.

Salazar Villegas, M. H., Qasim, M., Csaplovics, E., González-Martinez, R., Rodriguez-Buritica, S., Ramos Abril, L. N., & Salazar Villegas, B. (2023). Examining the Potential of Sentinel Imagery and Ensemble Algorithms for Estimating Aboveground Biomass in a Tropical Dry Forest. *Remote Sensing*, *15*(21), 5086. https://doi.org/10.3390/rs15215086

Sathasivam, S., Adebayo, S. A., Velavan, M., & Liang, J. K. W. (2022). Determine The Parameters for Photoelectric Effect Data Using Correlation and Simple Linear Regression. *Journal of Quality Measurement and Analysis*, *18*(3), 61–70. Scopus.

Sellaro, R., Crepy, M., Trupkin, S. A., Karayekov, E., Buchovsky, A. S., Rossi, C., & Casal, J. J. (2010). Cryptochrome as a Sensor of the Blue/Green Ratio of Natural Radiation in Arabidopsis. *Plant Physiology*, *154*(1), 401–409. https://doi.org/10.1104/pp.110.160820

Shinde, R. C., & Durbha, S. S. (2023). Adaptive LiDAR Reconstruction by Convolutional Compressive Sensing Network and Multivariate Empirical Mode Decomposition. *Signal Processing*, *213*, 109194–109194. https://doi.org/10.1016/j.sigpro.2023.109194

Subedi, P. B., & Zurqani, H. A. (2024). Estimating Above Ground Forest Biomass Using High-Resolution NAIP Imagery, Machine Learning, and Google Earth Engine. *2024 IEEE Asia-Pacific Conference on Geoscience, Electronics and Remote Sensing Technology (AGERS)*, 92–101. https://doi.org/10.1109/AGERS65212.2024.10932891

Tam, N. H., Loi, N. V., & Tuan, H. H. (2025). Establishing Models for Predicting Above-Ground Carbon Stock Based on Sentinel-2 Imagery for Evergreen Broadleaf Forests in South Central Coastal Ecoregion, Vietnam. *Forests*, *16*(4), 686. https://doi.org/10.3390/f16040686

Tang, F., & Xu, H. (2017). Impervious Surface Information Extraction Based on Hyperspectral Remote Sensing Imagery. *Remote Sensing*, *9*(6), 550. https://doi.org/10.3390/rs9060550

Tian, Z., Fan, J., Yu, T., De Leon, N., Kaeppler, S. M., & Zhang, Z. (2025). Mitigating NDVI saturation in imagery of dense and healthy vegetation. *ISPRS Journal of*

Photogrammetry and Remote Sensing, *227*, 234–250. https://doi.org/10.1016/j.isprsjprs.2025.06.013

Tilly, N., Aasen, H., & Bareth, G. (2015). Fusion of Plant Height and Vegetation Indices for the Estimation of Barley Biomass. *Remote Sensing*, *7*(9), 11449–11480. https://doi.org/10.3390/rs70911449

Tiruneh, G. A., Meshesha, D. T., Adgo, E., Tsunekawa, A., Haregeweyn, N., Fenta, A. A., & Reichert, J. M. (2022). A leaf reflectance-based crop yield modeling in Northwest Ethiopia. *Plos One*, *17*(6), e0269791–e0269791.

Tucker, C. J. (1979). Red and photographic infrared linear combinations for monitoring vegetation. *Remote Sensing of Environment*, *8*(2), 127–150. https://doi.org/10.1016/0034-4257(79)90013-0

Universitas Gadjah Mada. (2025, September 16). *Wanagama*. Fakultas Kehutanan, Universitas Gadjah Mada. https://wanagama.fkt.ugm.ac.id/wanagama-2/

Vélez, S., Martínez-Peña, R., & Castrillo, D. (2023). Beyond Vegetation: A Review Unveiling Additional Insights into Agriculture and Forestry through the Application of Vegetation Indices. *J*, *6*(3), 421–436. https://doi.org/10.3390/j6030028

Viljanen, N., Honkavaara, E., Näsi, R., Hakala, T., Niemeläinen, O., & Kaivosoja, J. (2018). A Novel Machine Learning Method for Estimating Biomass of Grass Swards Using a Photogrammetric Canopy Height Model, Images and Vegetation Indices Captured by a Drone. *Agriculture*, *8*(5), 70. https://doi.org/10.3390/agriculture8050070

Vogelmann, J. E., Rock, B. N., & Moss, D. M. (1993). Red edge spectral measurements from sugar maple leaves. *International Journal of Remote Sensing*, *14*(8), 1563–1575. https://doi.org/10.1080/01431169308953986

Wang, L., Guan, Y., & Li, X. (2024). Correlation and Simple Linear Regression. In X. Guo & F. Xue (Eds.), *Textbook of Medical Statistics* (pp. 157–170). Springer Nature Singapore. https://doi.org/10.1007/978-981-99-7390-3_11

Wei, Y., Lu, M., Yu, Q., Li, W., Wang, C., Tang, H., & Wu, W. (2024). The normalized difference yellow vegetation index (NDYVI): A new index for crop identification by using GaoFen-6 WFV data. *Computers and Electronics in Agriculture*, *226*, 109417–109417. https://doi.org/10.1016/j.compag.2024.109417

Xie, Q., Fu, W., Yan, W., Shi, J., Hao, C., Li, H., Xu, S., & Li, X. (2025). Research Analysis of the Joint Use of Sentinel-2 and ALOS-2 Data in Fine Classification of Tropical Natural Forests. *Forests*, *16*(8), 1302. https://doi.org/10.3390/f16081302

Xu, X., Liu, L., Han, P., Gong, X., & Zhang, Q. (2022). Accuracy of Vegetation Indices in Assessing Different Grades of Grassland Desertification from UAV. *International Journal of Environmental Research and Public Health*, *19*(24), 16793. https://doi.org/10.3390/ijerph192416793

Yue, Y., Zhao, W., & Liu, R. (2025). Relationships between vegetation indices and surface reflectance: Implications for detecting and monitoring sandification in arid regions. *Ecological Indicators*, *176*, 113640. https://doi.org/10.1016/j.ecolind.2025.113640

Zhang, Z., Lu, L., Zhao, Y., Wang, Y., Wei, D., Wu, X., & Ma, X. (2023). Recent advances in using Chinese Earth observation satellites for remote sensing of vegetation. *ISPRS Journal of Photogrammetry and Remote Sensing*, *195*, 393–407. https://doi.org/10.1016/j.isprsjprs.2022.12.006

Zhao, Y., Lee, C. K. F., Wang, Z., Wang, J., Gu, Y., Xie, J., Law, Y. K., Song, G., Bonebrake, T. C., Yang, X., Nelson, B. W., & Wu, J. (2022). Evaluating Fine-scale Phenology from PlanetScope Satellites with Ground Observations Across Temperate Forests in Eastern North America. *Remote Sensing of Environment*, *283*, 113310. https://doi.org/10.1016/j.rse.2022.113310

Zhen, Z., Chen, S., Yin, T., Chavanon, E., Lauret, N., Guilleux, J., Henke, M., Qin, W., Cao, L., Li, J., Lu, P., & Gastellu-Etchegorry, J.-P. (2021). Using the Negative Soil Adjustment Factor of Soil Adjusted Vegetation Index (SAVI) to Resist Saturation Effects and Estimate Leaf Area Index (LAI) in Dense Vegetation Areas. *Sensors*, *21*(6), 2115–2115. https://doi.org/10.3390/s21062115